Computer simulations reveal novel properties of the cell-cell signaling network at the shoot apex in /Arabidopsis

Pierre Barbier de Reuille, Isabelle Bohn-Courseau, Karen Ljung, Halima Morin, Nicola Carraro, Christophe Godin, Jan Traas

Computer simulations reveal novel properties of the cell-cell signaling network at the shoot apex in *Arabidopsis*.

Pierre Barbier de Reuille[*(1)], Isabelle Bohn-Courseau[†(1)], Karen Ljung[‡], Halima Morin[†], Nicola Carraro[§], Christophe Godin[¶(2)], Jan Traas[†‖(2)]

[*] INRA, UMR AMAP, TA40/PSII Bd de la Lironde, 34398 Montpellier Cedex 5, France

[†] INRA, Laboratoire de biologie cellulaire, Route de Saint-Cyr, 78026 Versailles cedex, France

[‡] Department of Forest Genetics and Plant Physiology, Umeå Plant Science Centre, SLU, S-901 83 Umeå Sweden

[§] Università Degli Studi Di Padova, Agripolis, Legnaro, 35020, Italy

[¶] INRIA, UMR AMAP, TA40/PSII Bd de la Lironde, 34398 Montpellier Cedex 5, France

[‖] New address: Laboratoire Reproduction et Développement des Plantes, ENS Lyon, 46 Allée d'Italie, 69364 Lyon, France

[(1)] These authors contributed equally to the work.

[(2)] Authors for correspondence. E-mail: jan.traas@ens-lyon.fr (J.T.) ; godin@cirad.fr (C.G.)

Abstract

The active transport of the plant hormone auxin plays a major role in the initiation of organs at the shoot apex. Polar localized membrane proteins of the PIN1 family facilitate this transport and recent observations suggest that auxin maxima created by these proteins are at the basis of organ initiation. This hypothesis is based on the visual, qualitative characterization of the complex distribution patterns of the PIN1 protein in *Arabidopsis*. To take these analyzes further, we investigated the properties of the patterns using computational modeling. The simulations reveal novel aspects of PIN1 distribution. In particular they suggest an important role for the meristem summit in the distribution of auxin. We confirm these predictions by further experimentation and propose a detailed model for the dynamics of auxin fluxes at the shoot apex.

Introduction

There is strong evidence that active auxin transport, generated by influx and efflux carriers, creates patterns of auxin distribution at the shoot apex. This distribution is, in turn, interpreted in terms of differential growth and cell differentiation (*1–3*). In *Arabidopsis*, AUX1, a putative influx transporter (*4*), is mainly located in the surface layer (L1) of the shoot apical meristem (*2*) (Figure 1A). Interestingly, the protein seems to be homogeneously distributed in plasma-membranes of the individual cells. Therefore it has been proposed that AUX1 helps to restrict auxin to these layers, although additional mechanisms may be required (*5*). The efflux facilitator PIN1 is also localized in the surface layers of the meristem, but in contrast to AUX1 it is often localized on certain anticlinal sides of the cells only. Since neighboring cells often show

coherent PIN1 positioning, it was proposed that PIN1 is responsible for directed hormone flows within the meristem L1 layer (Figure 1A). In particular, careful immunological studies have revealed that the membranes carrying PIN1 are preferentially oriented towards the incipient primordia, suggesting auxin transport towards the young organs (*2,3*).

Together the observations so far suggest a dynamic scenario where auxin is transported to the meristem from basally localized tissues via the L1 layer. At the meristem surface, auxin is redistributed and accumulates at particular sites where it will induce the initiation of new organs. This accumulation subsequently leads to the activation of transport in the provascular tissues causing an inward directed flow (Figure 1B, our own non-published results). The young organ is thus transformed into an auxin sink, which depletes its surroundings from auxin and prevents the formation of new primordia in its vicinity.

Although this scenario is relatively straightforward, the previous observations leave a number of questions open. First, it is not clear at all, why auxin should start to accumulate at the site where a primordium will be initiated. Second, the immunolabelings reveal a very complex distribution of PIN1 proteins (Figure 2). As a result the interpretation of these patterns in terms of cell-cell interaction networks and, more specifically, in terms of auxin distribution remains extremely difficult.

To address these questions, we developed computational modeling tools that allowed us to uncover novel aspects of the cell-cell interaction network and to predict auxin fluxes in the shoot apical meristems directly based on microscopical observations.

Material and methods

Immunolabeling of PIN1 protein

After embedding, the meristems were sectioned perpendicular to the main stems with a thickness of $12 - 15\mu$m. After labeling with anti-PIN1, the physical sections were viewed in the

confocal microscope to obtain an optimal image of the labeling patterns. In some cases, a single physical section was sufficient to cover the entire dome of the meristem. In other cases, the patterns of two successive sections were combined to cover the dome.

Anti-PIN1 Based on the sequence of *AtPIN1* (gene At1g73590), one potentially antigenic peptide sequence (GPTPRPSNYEEDGGPA) was selected in the large intra-cytosolic loop domain of AtPIN1 and used to produce antibodies (made by Eurogentec, Seraing, Belgium). This antibody recognizes PIN1, since no labeling is seen at the surface of the meristem in the *pin1* mutant. More detailed characterization of the antibody will be presented elsewhere. After immunostaining, the sections were viewed in a Leica confocal microscope to guarantee an optimal representation of the labeling patterns.

Gas chromatography and mass spectrometry (GCMS)

For GCMS, the plant tissue was collected in a 1.5 ml micro centrifuge tube and immediately frozen in liquid nitrogen. 0.5 ml cold 0.05 M phosphate buffer (pH 7.0) containing 0.02% sodium diethyldithiocarbamic acid (antioxidant) was added to the tube, together with $^{13}C_6$-IAA (Cambridge Isotope Laboratories, MA, USA) internal standard (50 pg/mg tissue) and a 3 mm tungsten-carbide bead. The sample was homogenized at 30 Hz in a vibration mill (Retsch MM 301, Haan, Germany) for 3 min, and then extracted under continuous shaking for 15 min at +4°C. After extraction, the pH was adjusted to 2.7 with 1 M HCl. Purification was performed using solid phase extraction on a 50 mg BondElut-C18 column (Varian, Middelburg, The Netherlands). The column was conditioned with 1 ml methanol, followed by 1 ml 1% acetic acid. After application of the sample, the column was washed with 1 ml 10% methanol in 1% acetic acid. The column was eluted with 1 ml methanol and the sample was then evaporated to dryness. 0.2 ml 2-propanol and 0.5 ml dichloromethane was added to the sample,

followed by 5 μL 2 M trimethylsilyl-diazomethane in hexane (Sigma-Aldrich, MO, USA). The sample was incubated in room temperature for 30 minutes, and excess diazomethane was then destroyed by adding 5 μL 2 M acetic acid in hexane. After evaporation to dryness, the sample was trimethylsilylated and analyzed by GC-SRM-MS as described.

Modeling tools

To interpret the labeling patterns in terms of putative auxin distribution, we developed a method relying on the simulation of auxin fluxes on digitized meristems.

Briefly, the method involves the following steps (Figure 3A-G). First the membranes of the individual cells are identified on the images of immunolabeled sections. This information is used to reconstruct a graph where the nodes represent the cells and every cell is connected to its neighbors. These connections are used to simulate auxin diffusion from cell to cell. A second type of connections is used to simulate active auxin transport. For this purpose, the cells are also connected via the membranes carrying PIN1 labeling. The latter connections are oriented (represented as arrows in figure 3D-E) to take into account the direction of PIN1 mediated efflux. Using these maps of interconnected cells, we simulated auxin transport applying a set of rules based on observations and hypotheses mostly taken from the literature (for a detailed description see supporting information).

To test the robustness of the auxin distribution patterns, we performed a range of tests in which only one parameter was modified at the time (specified in supporting information). For each test, the non-varying parameters were set to values intermediate between those having extreme effects on the simulation. The results showed that the patterns were qualitatively insensitive to major changes in diffusion and transport rates. At constant transport strength, the results were qualitatively equivalent for a thirteen-fold increase in diffusion rates. Conversely,

at constant diffusion rate, the results were qualitatively equivalent for a fivefold increase in transport strength. The patterns should, therefore, be considered as robust.

In a minority of the cells, the immunolabeling was not clear enough to assert the polarity or even the presence of the PIN-protein. Therefore, we classified the different connections into four categories with decreasing confidence level: strong signal (i), strong but unpolarized signal (ii), weak but polarized signal (iii), and weak and unpolarized signal (iv). We next performed the simulations removing the connections ii - iv. As the resulting patterns were not significantly different, we only considered the labeled membranes with the highest confidence level (for details see supporting information).

An aspect that was not taken into account was the relative level of immunolabeling. Since there is no experimental evidence of how this translates into transport rates, we restricted ourselves to recording only the presence/absence of PIN1 on cell walls.

Results

Simulation of auxin fluxes

The auxin transport through the network of interconnected cells was modeled using the following set of hypotheses:

1. Auxin passively diffuses via all walls (edges of the individual cells in the graph) and is actively transported via oriented connections only (*1–4, 6–9*). We only consider net auxin flux from cell to cell, without taking into account the molecular mechanisms involved (*5, 10–12*). To keep a tractable model at the tissue level, we decided to model this transport process using a simplified system, where we do not represent the compartment corresponding to the intercellular space. The net balance of auxin in a cell is thus considered to be the result of a direct exchange between cells through two processes: diffusion

from cell to cell and polarized active transport due to the presence of PIN1 molecules on certain walls of cells.

2. Auxin is restricted to the L1 layer and enters the meristem from the meristem border via the efflux facilitator (*2*), or alternatively, auxin injected intinjected into every cell within the meristem.

3. Auxin is evacuated via the L1 cells that are in contact with provascular strands characterized by PIN1 labeling in deeper layers (*1, 2*) (Figure 3G). Longitudinal sections show that these provascular strands are about three cells wide (not shown). Therefore a circular area of three cells wide is designated to evacuate auxin at the position of each provascular strand on the images. They are defined here as 'Primordia' (P-1, P-2, ..., P-1 being the nearest to the meristem summit) and behave as auxin sinks.

4. The simulation algorithm continues to distribute the virtual auxin in the system until the auxin distribution gets stationary. This is to take into account that the establishment of auxin distribution is a fast process, much faster than growth and cell proliferation (*2*). Therefore, in a normally growing meristem, auxin distribution is likely to be near the equilibrium at all times.

5. Cells cannot accumulate auxin indefinitely. We modeled this constraint using a saturation level, above which the cells no longer accept auxin influx. Simulations tests showed that this was not very different from the situation where, at high level of accumulation, auxin diffusion overcomes active transport (see supporting information).

6. Auxin is degraded at a constant rate in each cell. Situations with different degradation levels were tested, including no degradation at all.

Ten meristems that were precisely sectioned in a plane transverse to the stem were immunolabeled (*13*) using the PIN antibody. Subsequently the corresponding images were used to extract connection maps. When the 6 rules mentioned above were applied to these maps (for technical details see supporting information), virtual auxin accumulated at the sites where young primordia were being formed (Figure 3H-I). This property of the PIN1 network could be expected from visual inspection of the immunolabelings. However, the simulations also showed a strong accumulation of virtual auxin in a domain covering the meristem summit, a property not obvious from visual inspection only. In all meristems tested, the central zone of accumulation also locally extended further to the periphery. Interestingly, this peripheral protrusion corresponded precisely to the site where the organ founder cells of the next primordium (called here initium-1 or I-1) were expected. More specifically, the divergence angle between the last formed primordium and this initium oscillated between 105° and 145° with a mean at 130°. Extensive tests showed that the patterns were robust, relatively insensitive to even major changes in the parameters (see supporting information).

Auxin at the meristem summit

An unexpected simulation result was that the meristem summit accumulated auxin, suggesting a role for this domain in hormone distribution. Since previous studies only indicated a minor role for the meristem summit in this respect (*14*), we next tested this prediction in planta. We first analyzed plants expressing *GFP* under control of *pDR5*, a synthetic promoter that is sensitive to auxin and that has been used to estimate relative hormone threshold levels in different tissues (*3*). As expected, GFP was strongly expressed in the future organ primordia, even at very early stages of initiation i.e. at the level of I-1, just next to the meristem summit (Figure 4A; see also (*3*)). As a consequence, this pattern fully coincided with those predicted by the simulations. However, in contrast to what could be expected from the simulations, GFP was not, or very

weakly, expressed in the meristem summit. Therefore, either this domain contained little or no auxin, or *pDR5* was insensitive to auxin in the meristem summit. To distinguish between these two possibilities, we treated young *in vitro* grown plants (*15*) expressing *pDR5::GFP* with auxin in absence or presence of the auxin transport inhibitor NPA. The presence of 10^{-5}M auxin and 10^{-5}M NPA caused an important increase in the amount of *pDR5::GFP* expressing cells. However, the meristem summit never showed any increase in GFP activity, even in meristems where the entire periphery had activated the marker (Figure 4B-E). We concluded that, as judged by *pDR5* activity, the central domain of the meristem was auxin-insensitive.

The observed insensitivity did not provide any information on the actual amount of auxin present in this domain. To address this issue, we used a monoclonal antibody directed against auxin to define local differences in auxin concentrations (*16, 17*). This showed a weak, but consistent labeling pattern, with an obvious maximum at the meristem summit (Figure 4F-G).

To provide additional evidence that auxin did accumulate in the central part of the meristem, we extended our analysis to gas chromatography and mass spectrometry (GCMS, (*18,19*)). Since a normal wild-type meristem was too small to perform this type of analysis, we decided to use the *clavata3* (*clv3*) mutant. This mutant lacks a signaling peptide (CLV3) that is required to keep the central part of the meristem within certain size limits (*20, 21*). If this peptide is absent, the central domain continues to grow, until it is several millimeters wide (Figure 5A). To confirm that the central domain of the *clv3* meristem behaved like a normal wild-type meristem summit with regard to auxin sensitivity, we crossed the *pDR5::GFP* marker into the mutant background. In the enlarged dome of the mutant, we could only observe GFP fluorescence at the very periphery, close to the site of organ initiation (Figure 5B-C). The rest of the enlarged meristem did not express DR5-GFP. This confirmed that the auxin insensitive part of the meristem corresponded to the domain that is under control of the CLV3 pathway. This domain is believed to be equivalent to the so called 'central zone' required for meristem maintenance (*21*)

To determine whether the *clv3* summit did contain auxin or not, we next performed GCMS. For this purpose we measured the auxin contents in apices containing the SAM and young flower buds of *clv3* mutants. In addition, samples containing only cells coming from the enlarged meristematic summit of the *clv3* mutant were taken. The results (Figure 5D) showed that the samples enriched in central zone cells contained active IAA, and were even enriched in hormone. Thus, the hypothesis that the central domain of the meristem is insensitive to auxin, but contains free IAA, as suggested by the computer simulations and the auxin immunolabeling, was further confirmed using the IAA quantification in the *clv3* mutant. Several lines of evidence suggest that PIN1 is auxin inducible (*22*), which might seem in contradiction with our observation that PIN is expressed in the auxin insensitive center of the meristem. There are two possible explanations for this. First, PIN expression might also depend on other parameters than auxin and second, the meristem summit could be partially sensitive to auxin, via a pathway that does not involve the auxin responsive elements present in DR5.

Further simulation to test the role of auxin at the summit

What could be the function of IAA in the central domain of the meristem? To address this question, we performed additional simulations. These simulations were based on the same rules as before, but in addition the model was instructed to degrade auxin at the meristem summit. In all meristems tested, this additional instruction not only removed the auxin maximum from the meristem summit, but also the maximum at the level of the I-1 initium (Figure 6A-B). By contrast, the maxima around the formed primordia were maintained. The results, therefore, suggest that the meristem summit plays an essential role in the creation of novel auxin maxima at the site of the organ primordium founder cells.

Discussion

Together, the simulations and subsequent experiments lead to a model, in which auxin coming from the periphery is transported into the central zone of the meristem which is insensitive to the organ promoting effect of the hormone. At a certain level of accumulation, auxin can no longer freely enter the meristem summit and because new auxin is arriving constantly, the hormone will accumulate at the site where the fluxes towards the summit are the most abundant. In a way, this would be analogous to a "traffic jam" at the entry of the meristem. Our simulations predict that this site corresponds precisely to the I-1 area, i.e. the zone where the inter-primordium distance is the largest (Figure 7). At this stage, we have only considered the spiralled phyllotactic patterns observed in Arabidopsis. It will certainly be of interest to test our hypothesis that the model is also compatible with other types of phyllotaxis. For this purpose, more extensive simulation efforts using dynamic models will be required.

The results might seem in contradiction with elegant experiments where the tomato meristem summit was ablated using a laser (*14*). In this case, no modification in organ positioning was observed, at least for a period of up to 4-5 plastochrones, suggesting that the meristem center did not play an important role in organ positioning. To clarify this issue we performed additional simulations, where all cells from the meristem center were removed (Figure 6C). Interestingly, this did not have an effect on the accumulation of auxin at I-1 in the model. In this context, it should be noted that an ablated meristem center is analogous to a center which no longer accepts auxin. As a consequence, it would also cause an accumulation of auxin at the site where the fluxes are most abundant. Our results are, therefore fully compatible with the experimental evidence and provide an alternative explanation.

In this study, we have considered the molecular mechanism of auxin flux as a black box, which simply results in a net flux from cell to cell. Hereby, we assume that the PIN-labeled

membranes indicate the direction of active transport. Although we show that this approach can lead to testable hypotheses it might be of interest for the future to include certain processes or parameters that have remained inaccessible for our simulations. For example, it could be useful to consider chemical parameters such as pH dependent effects which influence permeability of auxin, or to include more precise information on auxin concentrations. For this purpose, it will be essential to develop the biological, mathematical and computer tools required to obtain and analyze quantitative information on these parameters.

In conclusion, our results reveal a robust network of cell interactions which is sufficient to generate auxin distribution patterns consistent with the observed organ positions (*23*). In addition they suggest a role for the meristem summit in organ positioning. The next, challenging step will now be to understand how the PIN1 proteins themselves are oriented. In this context, two major hypotheses have been proposed. In the first one, the patterns of cell polarity are due to the organization of local gradients of auxin concentrations. This hypothesis was originally used by (*10*) for designing a computational model of leaf venation formation and was used recently to model various types of leaf venation patterns (*24*). The phyllotaxis model developed by Jönsson *et al.* (*12*) is based on a similar hypothesis. In the second hypothesis, the orientation of PIN1 pumps results from a bio-chemical interpretation of mechanical stresses in the meristem surface. Such a mechanism would provide a possible molecular foundation for mechanical-based models (*25, 26*). By any means, it will not only be important to identify cellular mechanisms leading to polar localization of PIN1, but we need also to understand how these mechanisms are coordinated at the level of the whole meristem.

Acknowledgments. We would like to thank Przemyslaw Prusinkiewicz and Cris Kuhlemeier for critical reading of the text. We would also like to thank Jean-Louis Giavitto and Olivier Michel for providing the MGS language. We thank Jiri Friml for providing the *DR5::GFP* line.

P.BdR was financed by an ASC fellowship provided by INRA. J.T. was financed by an ACI from the french ministry of research and by the Marie Curie program of the EU. I.B-C was financed by the french ministry of research.

References

1. T. Vernoux, J. Kronenberger, O. Grandjean, P. Laufs, J. Traas, *Development* **127**, 5157 (2000).

2. D. Reinhardt, E.-R. Pesce, P. Stieger, T. Mandel, K. Baltensperger, M. Bennett, J. Traas, J. Friml, C. Kuhlemeier, *Nature* **426**, 255 (November 2003).

3. E. Benkova, M. Michniewicz, M. Sauer, T. Teichmann, D. Seifertova, G. Jurgens, J. Friml, *Cell* **115**, 591 (2003).

4. M. J. Bennett, A. Marchant, H. G. Green, S. T. May, S. P. Ward, P. A. Millner, A. R. Walker, B. Schulz, K. A. Feldmann, *Science* **273**, 948 (1996).

5. E. M. Kramer, *Trends Plant Sci.* **9**, 578 (Dec. 2004).

6. H. Vogler, C. Kuhlemeier, *Curr. Opin. Plant Biol.* **6**, 51 (2003).

7. L. Galweiler, C. Guan, A. Muller, E. Wisman, M. K., Yephremov, K. Palme, *Science* **282**, 2226 (1998).

8. D. Reinhardt, T. Mandel, C. Kuhlemeier, *Plant Cell* **12**, 507 (2000).

9. N. Carraro, A. Peaucelle, P. Laufs, J. Traas, *Plant Mol. Biol.* (Submitted).

10. G. J. Mitchison, *Proc. Roy. Soc. Lond. B* **207**, 79 (1980).

11. M. H. M. Goldsmith, T. H. Goldsmith, M. H. Martin, *Proceedings of the National Academy of Science of the USA* **78**, 976 (Feb. 1981).

12. H. Jönsson, M. Heisler, B. E. Shapiro, E. M. Meyerowitz, E. Mjolsness, *Submitted* (2005).

13. S. Vitha, F. Baluska, M. Mews, D. Volkmann, *J. Histochem. Cytochem.* **45**, 89 (1997).

14. D. Reinhardt, M. Frenz, T. Mandel, C. Kuhlemeier, *Development* **130**, 4073 (2003).

15. O. Grandjean, T. Vernoux, P. Laufs, K. Belcram, Y. Mizukami, J. Traas, *Plant Cell* **16**, 74 (January 2004).

16. O. Avsian-Kretchmer, J.-C. Cheng, L. Chen, E. Moctezuma, R. S. Z., *Plant Physiology* **130**, 199 (September 2002).

17. Monoclonal IAA antibody (Agdia, Elkart, Indiana, USA).

18. K. Ljung, P. Rishikesh, Bhalerao, G. Sandberg, *Plant Journal* **28**, 465 (2001).

19. A. Edlund, S. Eklöf, B. Sundberg, T. Moritz, G. Sandberg, *Plant Physiol.* **108**, 1043 (1995).

20. S. Clark, *Nat. Rev. Mol. Cell Biol.*, 276 (2001).

21. T. Laux, *Cell* **113**, 281 (2003).

22. A. Vieten, S. Vanneste, J. Wisniewska, E. Benková, R. Benjamins, T. Beeckman, C. Luschnig, J. Friml, *Development* **132**, 4521 (Oct 2005).

23. R. Lyndon, *The shoot apical meristem.*, (Cambridge University Press, 1998).

24. A. Runions, M. Fuhrer, B. Lane, P. Federl, A.-G. Rolland-Lagan, P. Prusinkiewicz.

25. P. Green, C. Steel, S. Rennich, (World Scientific, Singapore, 1998), pp. 359–392.

26. P. D. Shipman, A. C. Newell, *J. Theor. Biol.* **236**, 154 (Sept. 2005).

27. C. Thomas, R. Bronner, J. Molinier, E. Prinsen, H. van Onckelen, G. Hahne, *Planta* **215**, 577 (2002).

28. E. Moctezuma, J. F. Lewis, *Planta* **209**, 180 (1999).

29. R. H. Webb, *Rep. Prog. Phys.* **59**, 427 (Mar. 1996).

Figure 1: Models for auxin transport in the shoot apical meristem

(A) The putative auxin influx carrier AUX1, represented in black, is homogeneously distributed on the cell membranes of the surface layer of the meristem, while the putative auxin efflux carrier PIN1, represented in gray, seems to have a polarized localization. As proposed by (*2*), AUX1 would help to concentrate auxin in the surface layer (black arrows) and PIN1 would direct auxin fluxes (gray arrows) within these layers. Note that additional mechanisms responsible for auxin influx into the L1 layer have been proposed (*5*) .

(B) In the provascular tissues (*) of young primordia, PIN1 is oriented downwards, evacuating auxin from the meristem surface (orange arrows) to deeper tissues. Consequently, the primordia act as auxin sinks.

Figure 2: PIN1 immunolocalization in *Arabidopsis* shoot apical meristems (*13*)

(A) Global view of an anti-PIN1 immunolabeling on a meristem cross section. PIN1 is localized on the membrane and polarized in most cells. Patterns are complex. Bar, $20\mu m$.

(B) In the peripheral zone of the meristem, concentric PIN1 orientations around young primordia (asterisks) are observed. The patterns suggest that the cells orient towards a single central cell of the primordium.

(C) In boundaries between the meristem and the primordium, cell polarities in opposing directions are observed (arrows).

(D) At the meristem summit, PIN1 localization is variable and does not seem to show any particular organization. Bars, $10\mu m$.

Figure 3: From PIN1 immunolabeling to the simulation of auxin fluxes.

(A) A transverse section showing PIN-labeling. The rectangle indicates the detail shown in **(B)**. Merrysim (see supporting information) is used to capture the cell shapes and the PIN1 localization in each cell.

(C) All cell vertices (spots) are manually positioned. The vertices of each cell are subsequently grouped.

(**D**) Cells are manually connected to each other if and only if there is a PIN1 labeling on the membrane between them (arrows). The connection is oriented in the way of supposed PIN1-mediated efflux.

(**E**) The result is a network of cell interactions.

(**F** and **G**) Anti-PIN1 immunolabeling on two successive transverse sections of another meristem. In (G), the labeling of the provascular strands at the level of P1 and P2 can be clearly distinguished. At these positions, called the primordium centers, auxin will be evacuated in the simulations.

(**H** and **I**). Results of the simulated auxin fluxes in meristems shown in (A) and (F). The position of the primordium centers visible on the original images are marked by green and blue dots. Virtual auxin is injected via the black dots surrounding the meristems. The quantity of virtual auxin per cell is proportional to the red intensity. Auxin accumulates where young primordia are being formed but also at the meristem summit. Moreover, the auxin maximum at the meristem summit protrudes toward the initium I-1 (gray circle).

Bars, $20\mu m$.

Figure 4: Localization of auxin in *Arabidopsis* shoot apical meristems.

(**A** to **E**) Spatial pattern of *pDR5::GFP* expression in shoot apical meristems under different conditions.

(A) Untreated meristem. (B and C) Treatment of a meristem with 10^{-5} M IAA during 22 hours. 10^{-5} M NPA (auxin transport inhibitor) was added to keep auxin in the meristem (B: t=0h, C: t=22h). (D and E) Treatment of a meristem with 10^{-5} M of the synthetic auxin 2,4 D during 22 hours (D: t=0h, E: t=22h). The *pDR5::GFP* expressing domain covers a larger part of the periphery after the treatment with IAA-NPA or 2,4 D but the summit of the meristem remains unlabeled.

(**F** and **G**) Immunolocalization of IAA in shoot apical meristems (*27, 28*). The presence of labeling is characterized by a purple/brown signal.

(F) Cross section of a wild-type meristem; showing labeling at the meristem summit (arrow head). (G) Longitudinal section of a wild-type meristem also showing labeling at the meristem summit.

Bars, $20\mu m$.

Figure 5: Quantification of IAA in the central part of the *clv3* meristems.

(**A**) Schematic descriptions of wild-type and *clv3* meristems illustrating the enlarged central zone in *clv3* (CD: central domain). The green area represents the periphery domain (PD) where *pDR5::GFP* can be expressed.

(**B** and **C**) Pattern of *pDR5::GFP* expression in *clv3* meristems. (B) Global view of a full projection showing that *pDR5* activity is limited to the meristem periphery, with several maxima where the next primordia will be formed. (C) Detail of a meristem. Bars, $50\mu m$.

(**D**) Results of IAA quantification with GCMS in *clv3* meristems. Samples included the young apex (CD+PD+young primordia) or the central domain (CD) only. For each class, the quantification was performed on 4 different samples (4 triangles), each sample containing several meristems. The quantification shows that the central domain of *clv3* meristems concentrates significantly (at 1%) more IAA than the overall apex.

Figure 6: Testing the importance of auxin accumulation at the meristem summit.

(**A**) Simulation of auxin distribution using the standard parameter set (i.e. there are no special instructions for the meristem summit and auxin is evacuated only via the primordia P-1, P-2 and P-3).

(**B**) Simulation of auxin distribution in the same meristem, but this time the auxin arriving at the summit is immediately degraded. As a result, the maximum at the initium I-1 has disappeared.

(**C**) Simulation of auxin distribution in the same meristem, but this time, the meristem summit was removed. We defined this summit using the auxin accumulation zone. The initium I-1 is still present (A).

Figure 7: Auxin fluxes and primordium initiation.

(**A**, **B** and **C**) Auxin pathways inferred from a simulation (see supporting information). The color intensity in each cell is proportional to the contribution of this cell to auxin accumulation in the chosen zone (black: no contribution). The different zones are indicated as groups of colored dots.

(A) Auxin reaches the summit (gray dots) via corridors between primordia. The most important flux is between P-2 and P-3. I-1 is located at the limit of the summit and the most important flux towards the summit.

(B) The initium I-1 (yellow dots) is mainly filled by auxin coming from the periphery. PIN patterns suggest that the center contributes little.

(C) All three primordia receive auxin from the periphery. P-1 (red dots) and P-2 (blue dots) receive also some auxin from the center in contrast to P-3 (green dots).

(**D**) Model for the formation of an auxin maximum preceding creation of a primordium. As the distance between P-2 and P-3 increases, more auxin arrives at the meristem center in this sector. Since the center can only absorb a limited amount of auxin, this will lead to the formation of an auxin maximum (I-1). Eventually, this maximum will be transformed into a primordium (P-0) where the provascular system behaves as an auxin sink (black dot at the center of the primordium).

Bars, $20\mu m$.

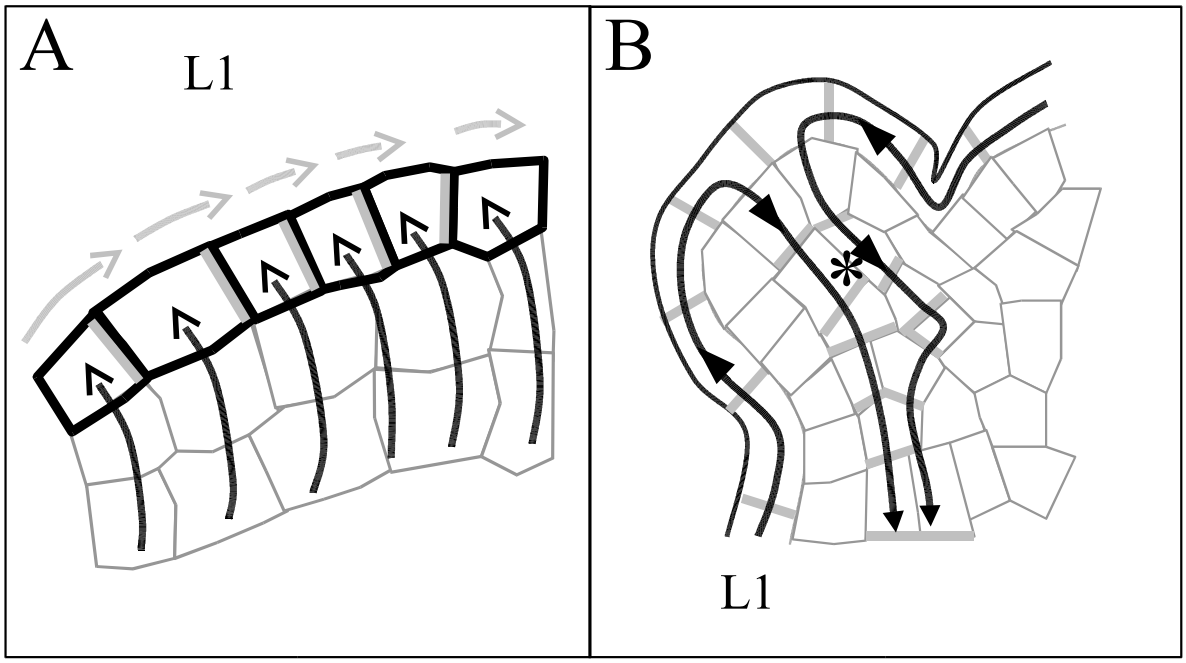

Figure 1

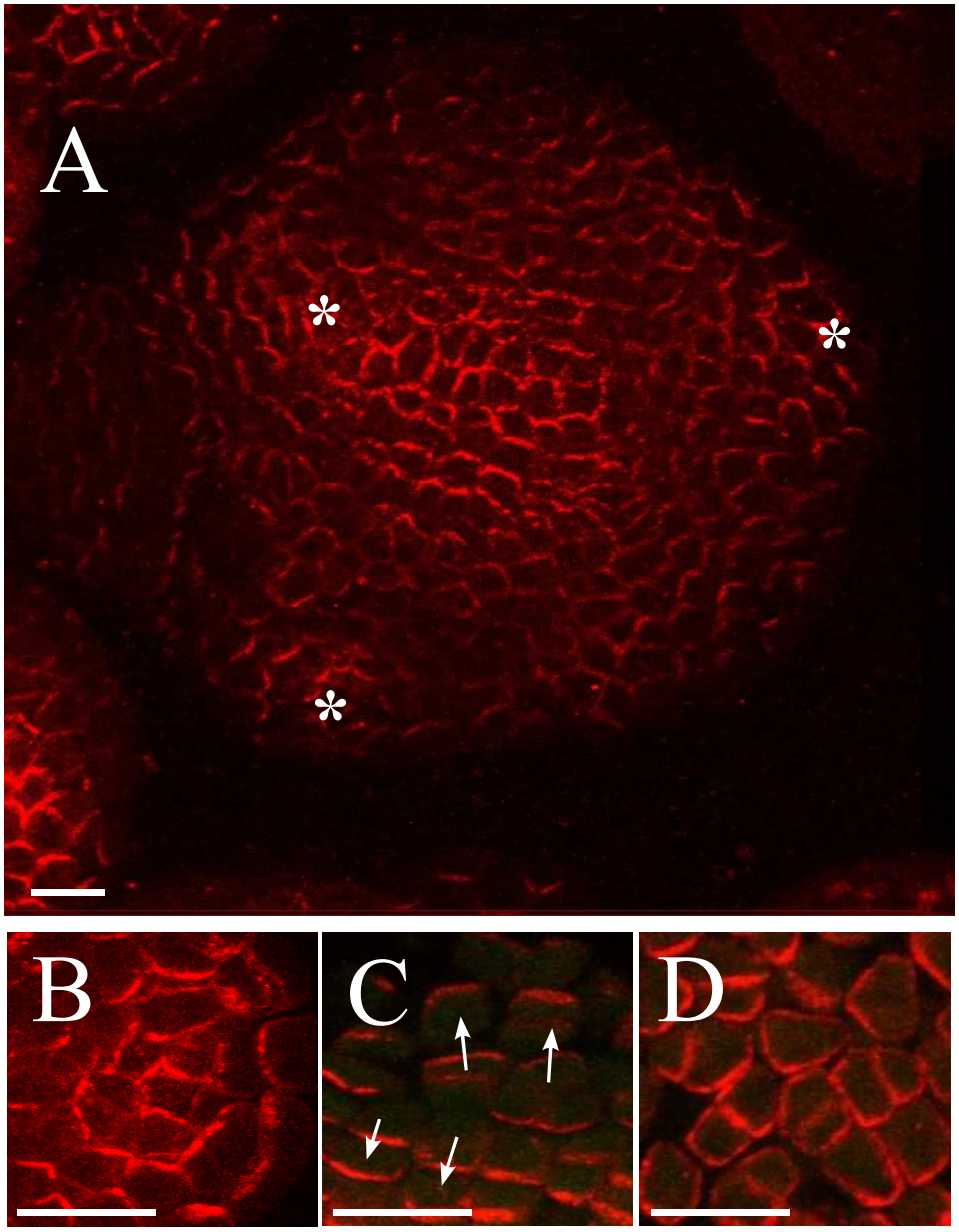

Figure 2

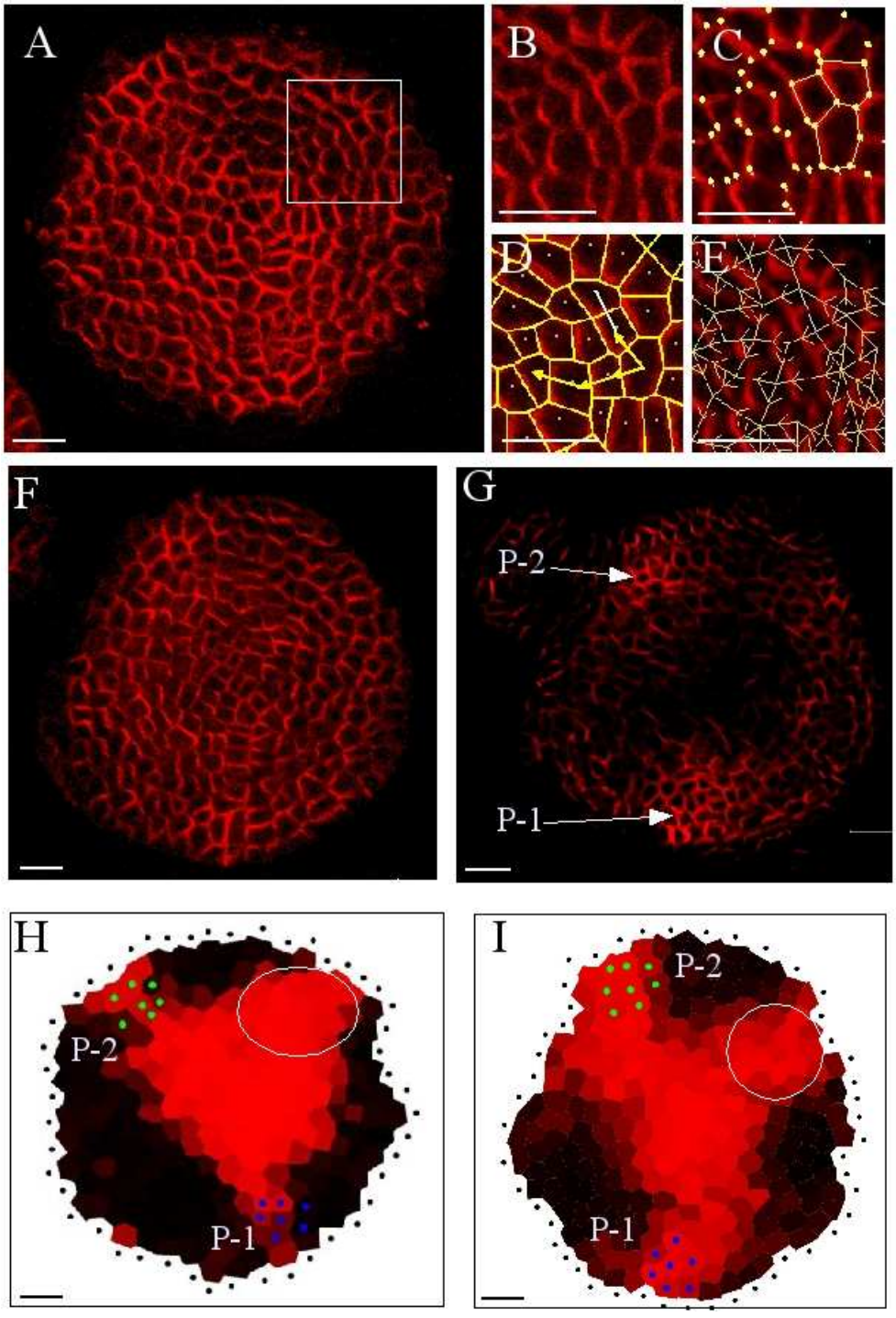

Figure 3

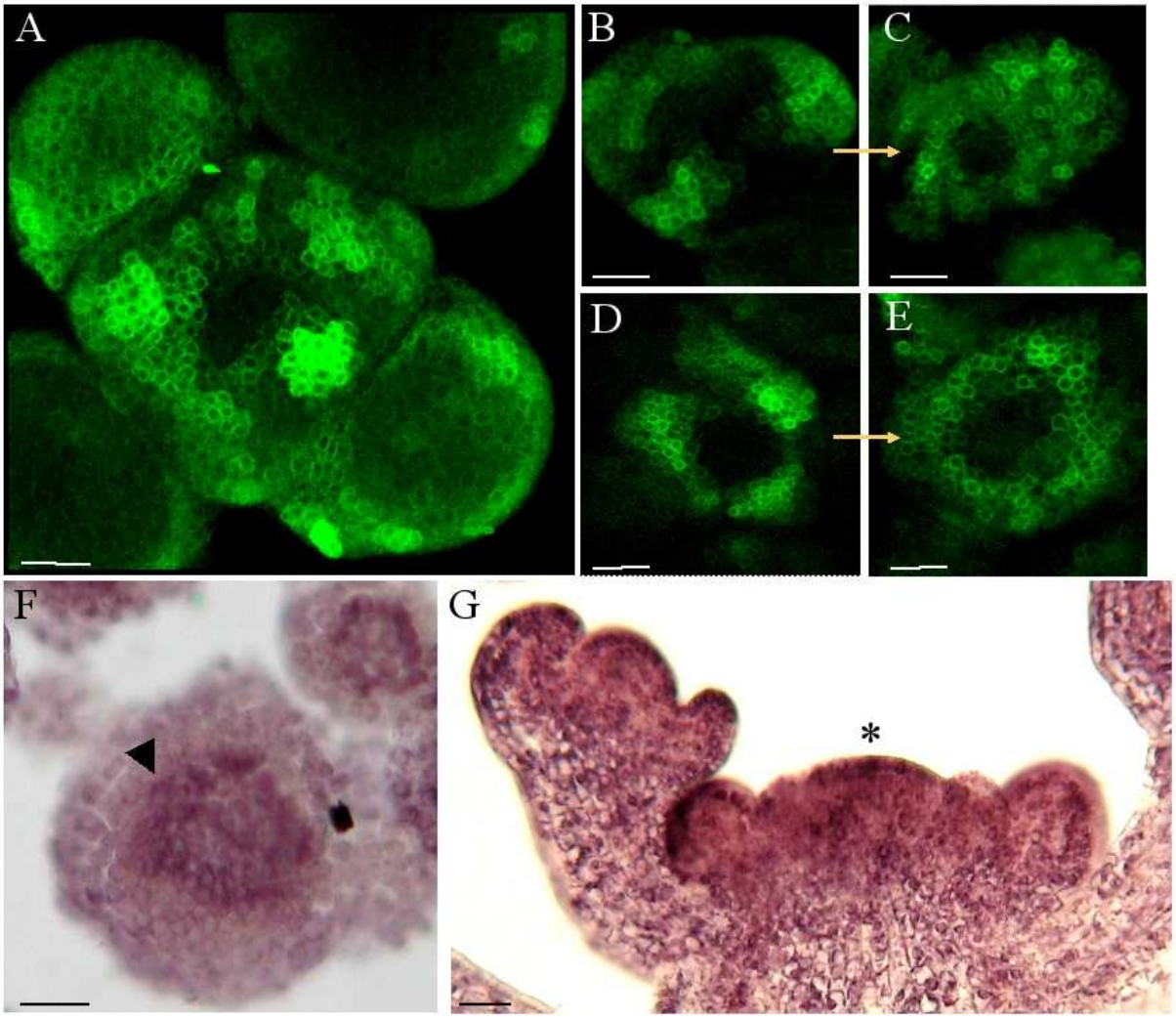

Figure 4

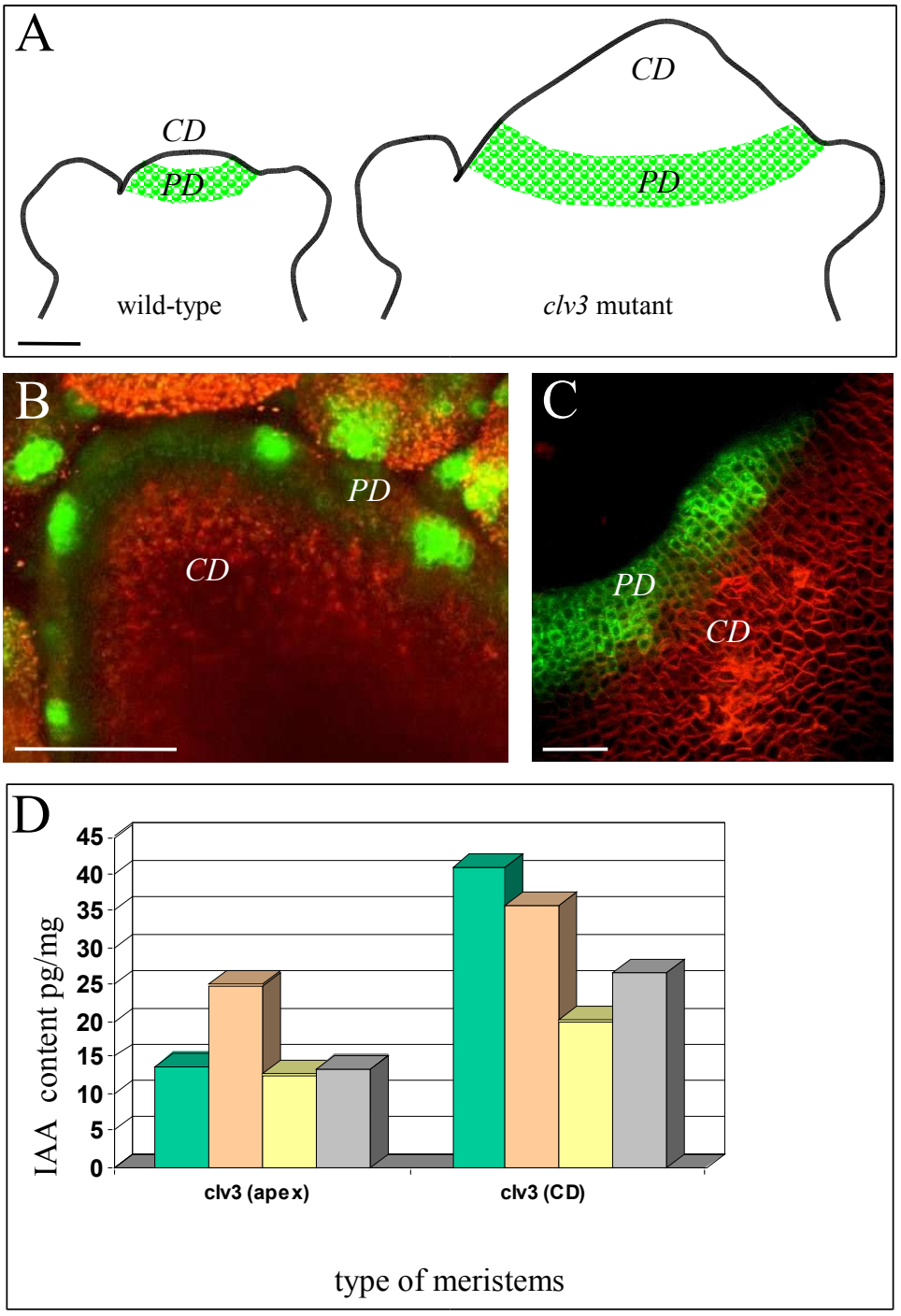
A
CD
PD
wild-type
CD
PD
clv3 mutant
B
PD
CD
C
PD
CD
D
IAA content pg/mg
45
40
35
30
25
20
15
10
5
0
clv3 (apex)
clv3 (CD)
type of meristems

Figure 5

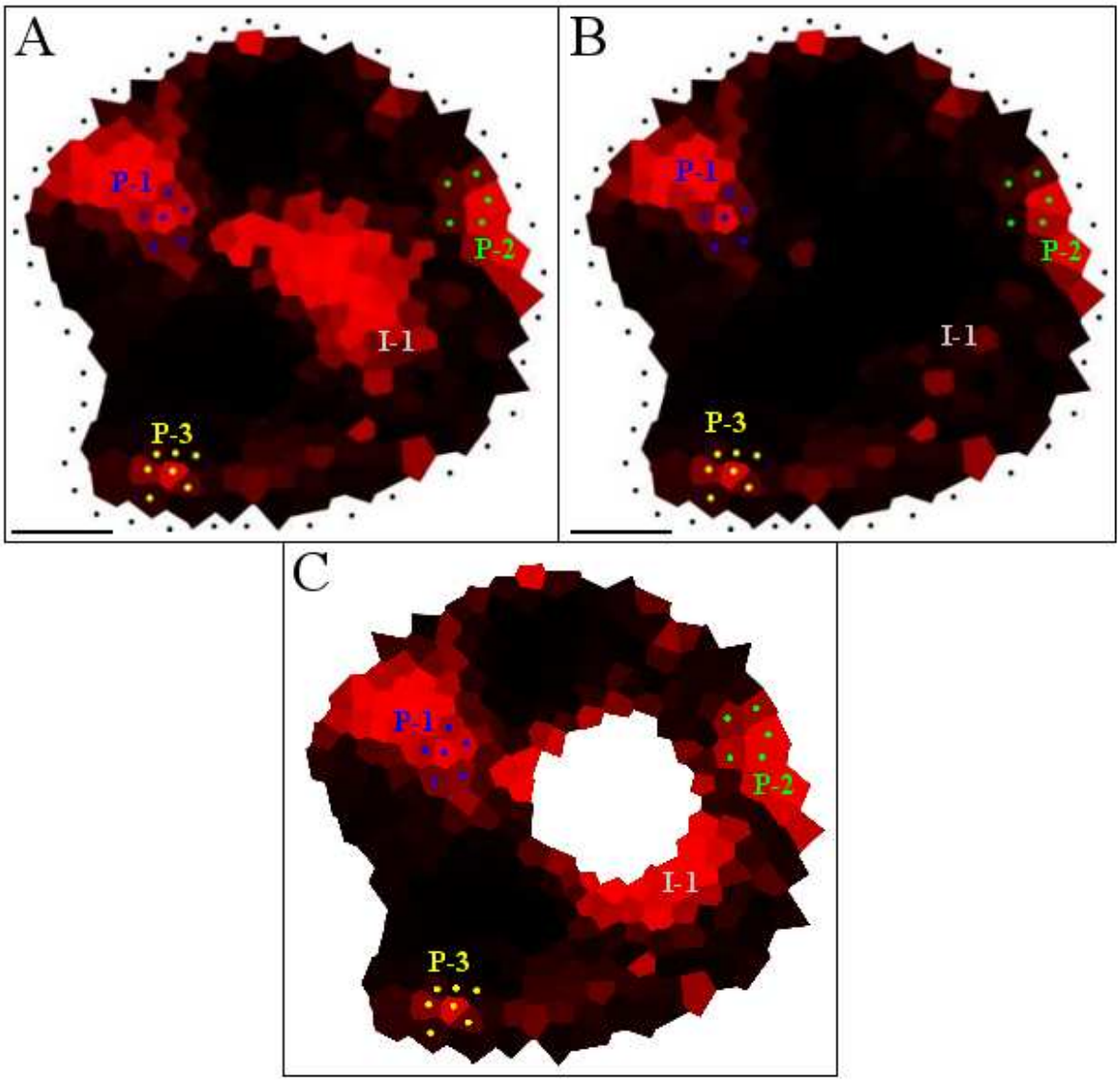

Figure 6

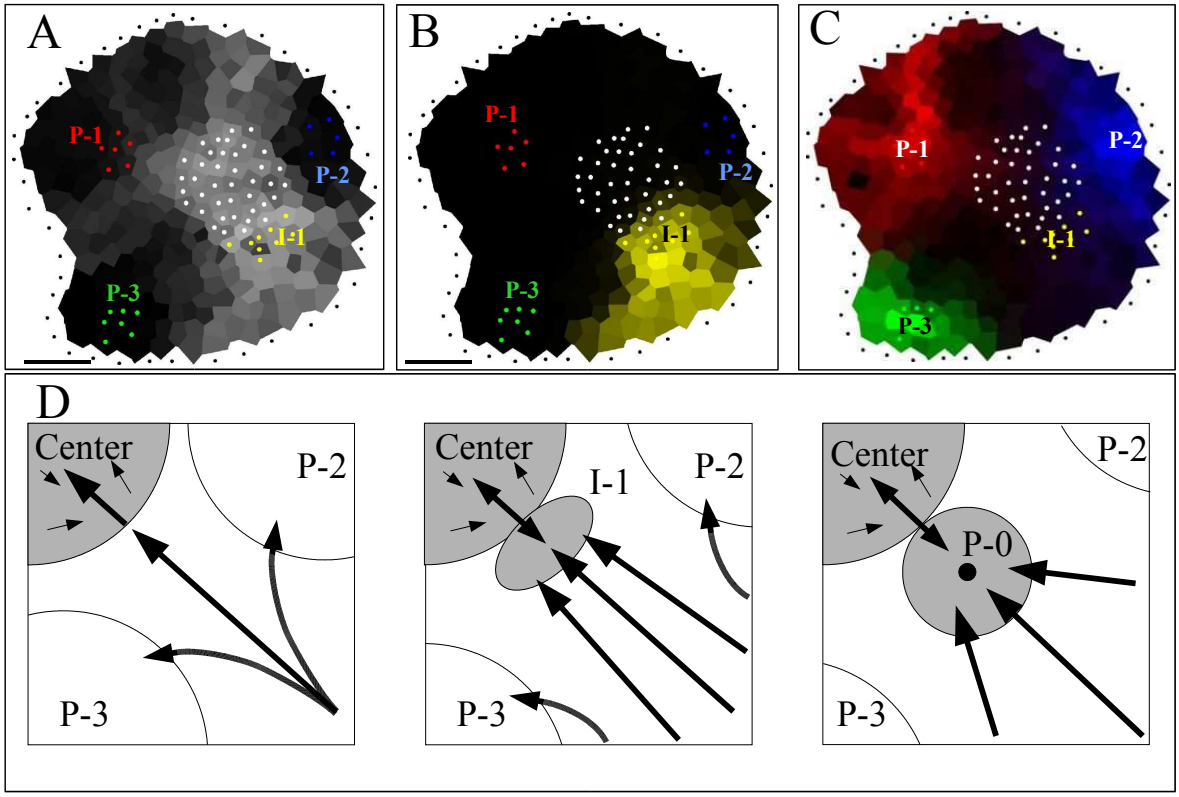
A
P-1
P-2
I-1
P-3
B
P-1
P-2
I-1
P-3
C
P-1
P-2
I-1
P-3
D
Center
P-2
P-3
Center
I-1
P-2
P-3
Center
P-2
P-0
P-3

Figure 7